Mechanism of Calcium Fluoride Acceleration for Vacuum Carbothermic Reduction of Magnesia

CrossMark

YUN JIANG, YU-QIN LIU, HONG-WEN MA, and WEI-GONG ZHOU

The use of a small amount of calcium fluoride as an additive greatly accelerated the reduction of magnesia during the preparation of magnesium from magnesia using the vacuum carbothermic reduction method. At 1573 K (1300 °C), the magnesia reaction rates of the samples with 1, 3, and 5 pct CaF_2 were all approximately 26 pct, three times that of free CaF_2, and they were arranged in order of the calcium fluoride weight percentages at 1673 K (1400 °C). The residues were analyzed using chemical analysis, XRD, SEM, EDS, and XRF. The possible acceleration mechanism was discussed. Calcium fluoride combined with magnesia and silicon dioxide to form a eutectic that melted as a channel to aid the solid–solid reaction between carbon and magnesia at approximately 1573 K (1300 °C). Calcium fluoride in the molten state offered free calcium ions and fluorine ions. Fluorine ions entered and distorted the magnesia crystal lattice. The structural strength and chemical stability of the magnesia crystal lattice decreased, which facilitated the magnesia reduction by carbon. Calcium ions were employed to generate the calcium and magnesium silicate. The easily evaporating fluorides, including magnesium fluoride and silicon tetrafluoride, were regarded as the main reason for the loss of fluorine.

I. INTRODUCTION

CALCIUM fluoride has been widely used as a reaction accelerator in ferroalloy production and ferrous metallurgy, including magnesium metallurgy.[1–8] During the industrial production of magnesium using the Pidgeon process in China, calcium fluoride may be added at a nominal rate of 0.2 kg per 1 kg of pure magnesium.[9] Calcium fluoride also obviously enhances the reaction rate of magnesia in the preparation of magnesium using vacuum carbothermic reduction method.

Based on the previous thermodynamic analysis, the carbothermic reduction reaction is

$$MgO_{(s)} + C_{(s)} = Mg_{(g)} + CO_{(g)}. \qquad [1]$$
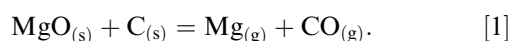
The reaction between magnesia and carbon produces magnesium vapor and carbon monoxide. The gaseous mixture is cooled down when it is pulled out from the heating system. The magnesium vapor condenses on the surface of the condenser, and carbon monoxide is expelled from the equipment. The system pressure affects the reaction because solid materials transform into gaseous products during the reaction. The decrease of the system pressure contributes to the forward reaction. The thermodynamic calculation indicates that the beginning reaction temperature dips to 1387 K (1114 °C) when the system pressure in the vacuum oven is 20 Pa.[10]

Some experiments on the vacuum carbothermic reduction of magnesia with various amounts of calcium fluoride have been performed. Li[11] noted that the rapid reaction temperature without CaF_2 is approximately 1750 K (1477 °C) at 150 Pa. Tian[12] confirmed that the reaction with 5 pct CaF_2 at 30 to 100 Pa is sharply accelerated only at 1573 K (1300 °C). Gao[13] observed that the magnesia reaction rate with 5 pct CaF_2 at 1673 K (1400 °C) for an hour increased from 31.02 to 91.72 pct. However, the mechanism of calcium fluoride in the experiment is not fully clear and remains worthy of investigation. Therefore, experiments and analyses have been conducted to investigate the effect and mechanism of calcium fluoride on the reaction.

II. EXPERIMENTS

A series of experiments were performed. The raw materials were magnesia, coke, and calcium fluoride. Light magnesium oxide and calcium fluoride, produced by the Sinopharm Chemical Reagent Co., Ltd., were both analytical reagent with nominal purities of 98.0 and 98.5 pct, respectively. Senior grade metallurgical coke with some complex components produced in Shanxi, China, was used as the reductant. The chemical compositions of magnesia, coke, and calcium fluoride are listed in Tables I, II, and III, respectively.

YUN JIANG, Lecturer, is with the School of Science, China University of Geosciences, 29 Xueyuan Road, Haidian District, Beijing 100083, China. YU-QIN LIU, Associate Professor, and HONG-WEN MA, Professor, are with the School of Materials Science and Technology, China University of Geosciences, 29 Xueyuan Road, Haidian District, Beijing 100083, China. Contact e-mail: mahw@cugb.edu.cn WEI-GONG ZHOU, Associate Professor, is with the Great Wall College, China University of Geosciences, 1698 South Second Ring Road, Baoding 071000, China.

Table I. Chemical Composition Analysis Results of Light Magnesium Oxide (w_B/pct)

Item	SiO_2	Al_2O_3	Fe_2O_3	TiO_2	CaO	MgO	K_2O
Content	0.06	0.03	0.01	0.02	0.02	98.07	0.01

Item	Na_2O	MnO	SO_3	P_2O_5	H_2O-	Loss of Ignition	
Content	0.06	0.00	0.02	0.00	0.00	1.78	

Table II. Chemical Composition Analysis Results of Coke (w_B/pct)

Item	M, ad	A, ad	V, ad	FC, ad	FC, d	Coke Cinder Character
Content	0.22	14.74	1.46	83.58	83.67	2

Item	SiO_2	Al_2O_3	Fe_2O_3	TiO_2	CaO	MgO
Content	45.40	33.18	10.57	1.62	3.44	0.75

Item	K_2O	Na_2O	MnO	SO_3	P_2O_5	
Content	0.80	0.42	0.19	2.05	0.28	

Note: 'M,ad' is the total moisture content of the raw coke sample, 'A,ad' is the ash content, 'V,ad' is the volatile content, 'FC,ad' is the fixed carbon content, and 'FC,d' is the fixed carbon content of the dried coke sample. 'Coke cinder character' describes the residues' shape and property after the determination of volatiles, and the coke cinder characteristic code '2' indicates that it was adhesive and the larger mass more easily became a powder with gentle touch. The items after SiO_2 (including SiO_2) represent the chemical composition analysis of ash (A,ad).

Table III. Chemical Composition Analysis Results of Calcium Fluoride (w_B/pct)

Item	CaF_2	Loss of Ignition	Chloride	Sulfite	Total Nitrogen
Content	≥98.5	≤0.4	≤0.01	≤0.05	≤0.005

Item	Fluorosilicate	Phosphate	Fe	Heavy Metal	
Content	≤0.01	qualified	≤0.003	≤0.003	

Note: Because of the difficulty in the CaF_2 analysis, the data in the table are the nominal values.
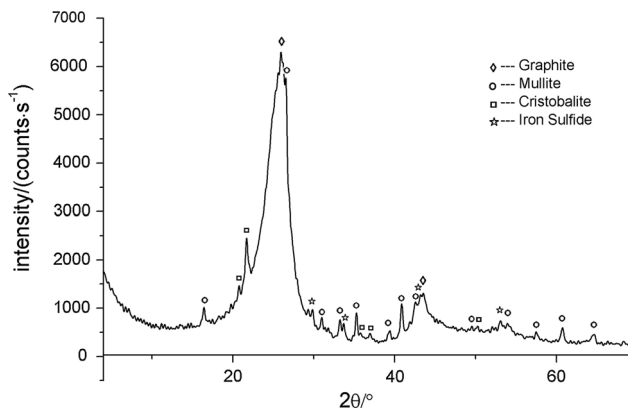

Fig. 1—XRD pattern of coke.

The X-ray diffraction (XRD) analysis result of coke is shown in Figure 1. The fixed carbon in the sample was 83.58 pct and remained in the phase of amorphous carbon and graphite crystallite, appearing as a raised bulge corresponding to the graphite peak. The main ingredients in its ash were silica and alumina, which existed as the mullite phase ($Al_6Si_2O_{13}$) and cristobalite phase (SiO_2).

To ensure calcium fluoride's impact on the reducing process, a group of contrast experiments were conducted. The coke and light magnesium oxide were mixed evenly based on the molar ratio of carbon and magnesia (1.2). The mass percentages of silica and alumina in the total mixture were 2.20 and 1.61 pct, respectively. Other substances, including iron oxide, made up less than 0.52 pct and had little effect; thus they were not considered. The powder was divided in quarters; 1, 3, and 5 wt pct CaF_2 was added to three of the quarters, and the remaining quarter was left free of CaF_2. The four parts were separately ground, mixed evenly again, and pressed into pellets with diameters of 40 mm using a pressure of 20 MPa. The four types of pellets were named RS0, RS1, RS3, and RS5 according to the addition of calcium fluoride.

The shaped samples were placed into a vacuum oven. The oven was closed, and a vacuum pump was used to reduce the system pressure. Heating began until the system pressure

reached 5 Pa. The first series of experiments examined the effect of temperature. The reactions lasted 60 minutes at 1373 K, 1473 K, 1573 K, and 1673 K (1100 °C, 1200 °C, 1300 °C, and 1400 °C). Another series of experiments examined the effect of reaction time. The reactions occurred in 1673 K (1400 °C) for 0, 30, 60, and 90 minutes. The system pressure rose to approximately 20 Pa during the heating stage and ranged stably from 20 to 8 Pa when the temperature was maintained at a certain level. All of the residues were analyzed using the chemical method, and some of them were examined using X-ray diffraction (XRD), X-ray fluorescence (XRF), and scanning electron microscopy (SEM).

III. ANALYSIS AND RESULTS

The raw sample kept its pellet shape but shrank successively during the reaction. When the sample did not fully reacted, the residue has an ash layer with the radius of R_O outside after the gas product left and an unreacted hard core inside with the radius of R_I. With time lasting or temperature rising, the sample became completely dark gray porous fragile ash bulk, in which there was still less carbon and magnesia. During the process, the radius was becoming smaller from the raw sample's R_S to the ash bulk's R_A. Figure 2 shows the reaction process.

A. Reaction Rate of Magnesia

The reaction rate of magnesia is calculated using the following formula:

$$\beta = \frac{W_0 - W_1}{W_0} \times 100 \, \text{pct} = \frac{\alpha_0 \times m_0 - \alpha_1 \times m_1}{\alpha_0 \times m_0} \times 100 \, \text{pct},$$

[2]

where W_0 is the magnesia mass before reduction, which is obtained using the formula $W_0 = \alpha_0 \times m_0$, in which α_0 is the weight percent of magnesia and m_0 is the total mass of the reactants. W_1, α_1, and m_1 correspond to the mass of magnesia, the weight percent of magnesia, and the total mass of the residue after the reduction, respectively.

Figure 3 shows the relation between the reaction rate and weight percentage of CaF_2. In Figure 3(a), the reaction rates were almost the same at 5 pct at 1373 K

(1100 °C) or lower, indicating that the reduction reaction between coke and magnesia did not occur. At 1473 K (1200 °C), the reaction rates changed slightly. At 1573 K (1300 °C), the reaction rates of the reactants with CaF_2 were similar (25.20, 27.00, and 26.81 pct) regardless of the weight percentages of calcium fluoride. It was three times that of free CaF_2 (9.52 pct). At 1673 K (1400 °C), the reaction rates were arranged in order of weight percentage of CaF_2 at 43.70, 52.51, and 61.60 pct. Their reaction rates were approximately double that without CaF_2 (26.14 pct).

In Figure 3(b), the reaction rates of magnesia at 1673 K (1400 °C) were arranged in order of weight percentage of CaF_2 for a reaction time of 90 minutes. These values were obviously higher than that of RS0. The reaction rates of RS0 increased linearly with time, whereas those of the samples containing CaF_2 slowed down with the same trend when the reaction time lasted more than 30 minutes because at 30 minutes, the gap between RS1 and RS0, RS3 and RS0, and RS5 and RS0 were maintained at approximately 16, 25, and 33 pct, respectively, with no obvious change. The difference occurs when the reaction temperature increases from 1573 K to 1673 K (1300 °C to 1400 °C) and when the time is less than 30 minutes.

B. X-ray Diffraction Analysis

The comparison group's residues were analyzed to identify the phase transition in each stage of the reaction. The XRD spectrum of the raw samples and residues are shown in Figure 4. The raw samples, RS0, RS1, RS3, and RS5, were named based on the addition of calcium fluoride. The residues were named according to the experiment conditions and the addition of calcium fluoride. For example, the code 1473603 indicates that the residue came from the sample with 3 wt pct CaF_2 that had reacted at 1473 K (1200 °C) for 60 minutes (the first four numbers are the reacting temperature, the next two are the reacting time, and the last one is the weight percentage of CaF_2 in the sample).

In Figure 4, mullite ($Al_6Si_2O_{13}$) and cristobalite (SiO_2) always disappeared, and the spinel ($MgAl_2O_4$) and olivine (Mg_2SiO_4) appeared after the samples were heated at 1473 K (1200 °C) for 60 minutes.

For the samples containing CaF_2, the calcium fluoride peaks increased with the weight percentage of CaF_2. When the reaction temperature increased, the calcium
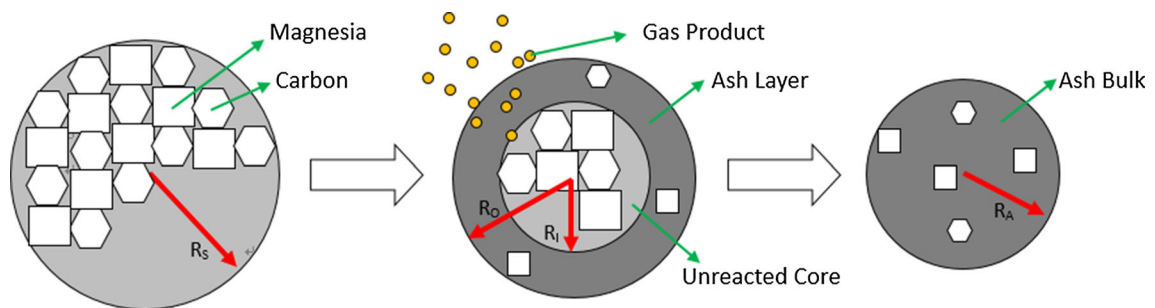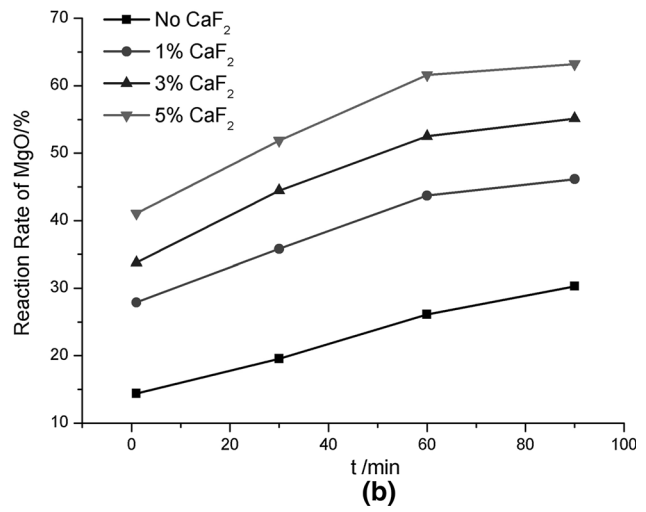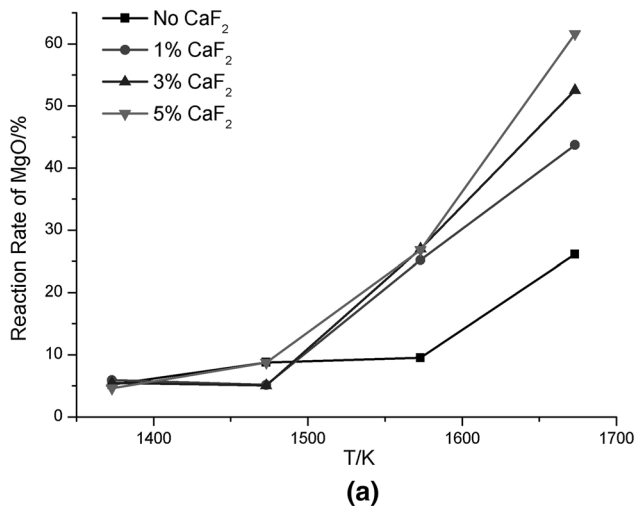

Fig. 2—Status of raw sample and residue.

Fig. 3—Magnesia reaction rate change as a function of weight percentage of CaF₂. (*a*) Effect of temperature (60 min) and (*b*) effect of time [1673 K (1400 °C)].
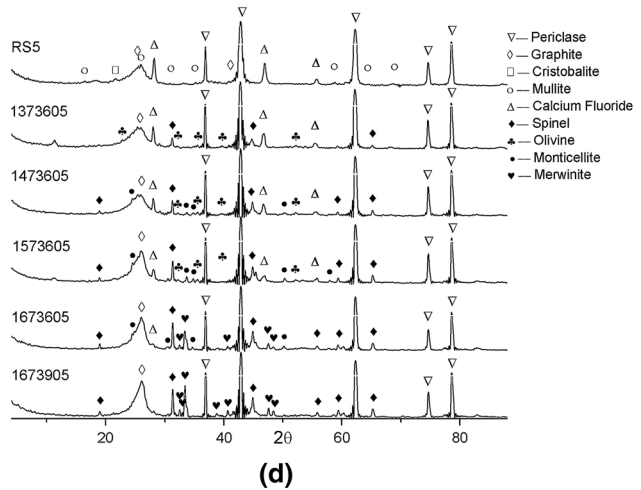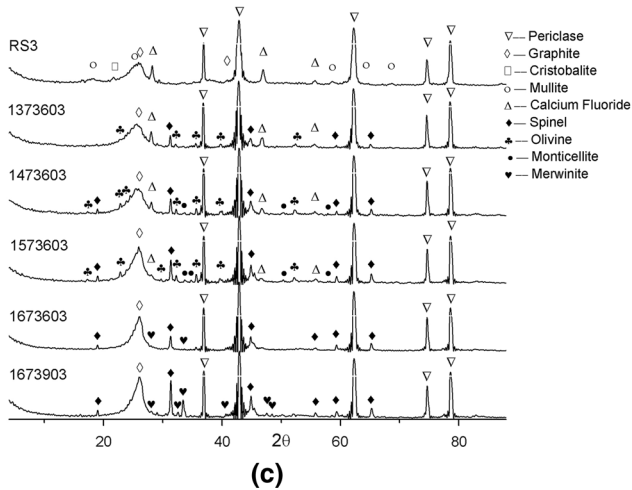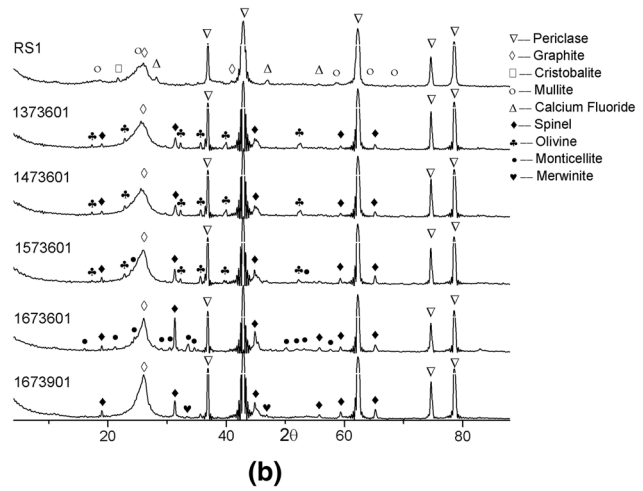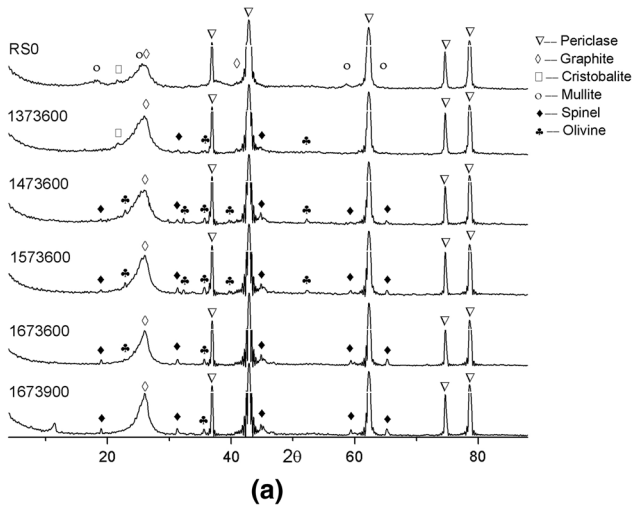

Fig. 4—XRD patterns of raw samples and residues under various experiment conditions. (*a*) RS0 and its residue, (*b*) RS1 and its residue, (*c*) RS3 and its residue, and (*d*) RS5 and its residue.

fluoride peaks generally decreased and eventually vanished. When less calcium fluoride was added, the peaks disappeared more quickly.

The olivine phase (Mg_2SiO_4) appeared at 1373 K (1100 °C) in all of the samples. For sample RS0, the olivine phase was present at every reaction temperature. For RS1, RS3, and RS5, the olivine phase was present from 1373 K to 1573 K (1100 °C to 1300 °C) and was then replaced by other phases containing calcium.

The monticellite phase ($CaMgSiO_4$) did not appear until 1573 K (1300 °C) for sample RS1, reached a high level when the sample was heated at 1673 K (1400 °C) for 60 minutes, and then disappeared after 90 minutes. For samples RS3 and RS5, the phase appeared at 1473 K (1200 °C) and reached its highest level at 1573 K (1300 °C). The phase vanished in RS3 and was still present in RS5 when the temperature reached 1673 K (1400 °C). The addition amount of CaF_2 determined the duration that the monticellite phase remained in the samples.

The merwinite phase ($Ca_3Mg(SiO_4)_2$) appeared at 1673 K (1400 °C) for 90 minutes for RS1 and at same temperature for 60 minutes for RS3 and RS5. For a higher CaF_2 weight percentage, the merwinite phase appeared earlier.

C. X-ray Fluorescence Analysis

Several elements, including calcium, silicon, fluorine, and aluminum, were the second main elements except the carbon and magnesium for the raw samples. The residues of RS3 were ground and analyzed using the X-ray fluorescence method. The weight loss percentages of the elements were calculated and are shown in Figure 5. The loss of fluorine increased progressively with an increase in the reaction temperature. A loss of 92.4 pct fluorine occurred at 1673 K (1400 °C) after 60 minutes, and the fluorine vanished after 90 minutes. The weight of the other three elements changed less when the reaction temperature was below 1573 K (1300 °C); however, their loss almost doubled at 1673 K (1400 °C), especially that of silicon (57.7 pct).

D. Scanning Electron Microscope and Energy Spectrum Analysis

The SEM images in Figure 6 show the surface details of the samples. Figure 6(a) shows the sample before the reaction, in which the large gray bulk represents the unbroken coke with a relatively neat edge, whereas the white fine particles are a mixture of the magnesia and a small account of calcium fluoride. Figure 6(b) shows the residue after the reaction at 1473 K (1200 °C) for 60 minutes. The coke edge is still neat. The mixture combined more tightly than before. Figure 6(c) shows the residue after the reaction at 1573 K (1300 °C) for 60 minutes. The gray flakes are coke with a coarse surface and toothed edge. The magnesia grew into larger spherical particles, approximately 1 μm, combined together, and some caves appeared. The cross-linker in the middle is thought to be a type of silicate based on its crystal shape. The phenomenon indicated that the
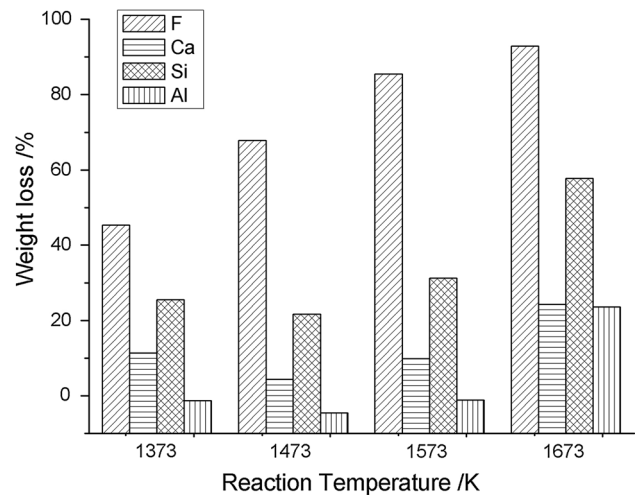

Fig. 5—Weight loss percentage of elements in RS3 at various reaction temperatures.

materials began to react fast at 1573 K (1300 °C). Figure 6(d) shows how the spherical particle's size continued to grow to approximately 3 μm and blurred the grain boundary. The scattered debris is the ash of coke. The cave increased in size because of the consumption of reactants.

The cemented parts in residues 1473603 and 1573603 were probed by EDS. Figure 7 shows the probed area, and Table IV lists the micro-area atomic percentage. The cemented part of 1473603 contained seven elements, including C, Mg, O, Ca, F, Si, and Al, and the magnesium and oxygen contents were 40.36 and 46.74 pct, respectively. Fluorine and calcium still coexisted in 1473603 even if their atomic proportion was 1.72, which is higher than that of calcium fluoride, 0.5. In the cemented part of 1573603, the magnesium and oxygen contents dipped to 14.81 and 9.35 pct, respectively. The calcium atomic percent reached 26.25 pct; however, the fluorine atomic percent, with silicon and aluminum, became zero.

IV. DISCUSSION

The experiments demonstrated that calcium fluoride plays an important role in the vacuum carbothermic reduction of magnesia. Comparison of the reaction rates of magnesia with different amounts of calcium fluoride, shown in Figure 3, suggests that the CaF_2 does not lower the initial temperature of reduction [1387 K (1114 °C) theoretically]. Only when the reaction begins, the acceleration of calcium fluoride makes the reaction rates distinct.

According to the above experimental results, RS1, RS3, and RS5 have similar reaction rates at 1573 K (1300 °C) after 60 minutes and have the same reaction rate growth at 1673 K (1400 °C) when the time is longer than 30 minutes. The amount of CaF_2 shows its effect when the temperature ranges from 1573 K to 1673 K (1300 °C to 1400 °C). Higher weight percentages of CaF_2 result in higher reaction speeds. Therefore, the
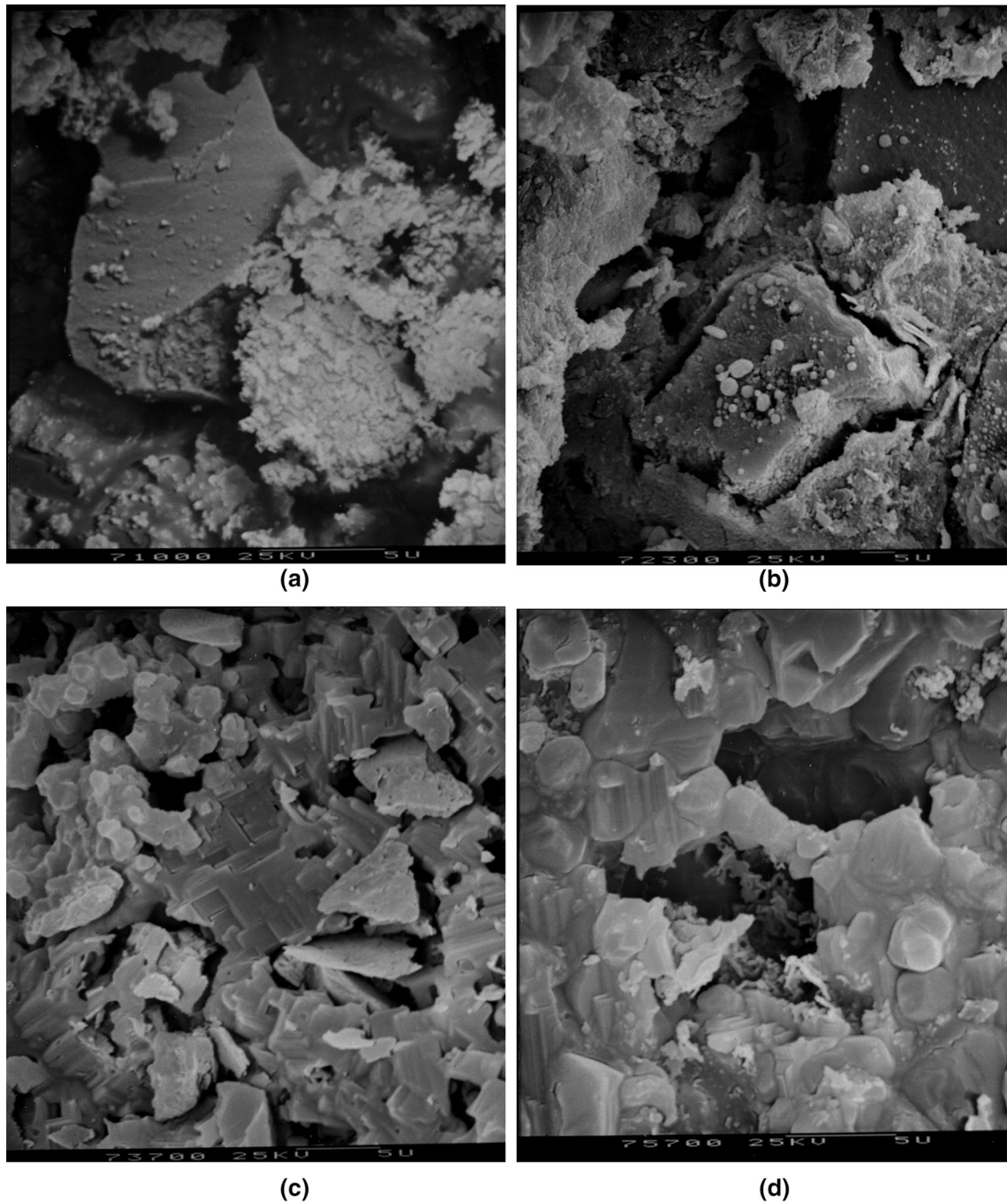
Fig. 6—SEM images of RS3 and its residues after 60 min. (*a*) RS3, (*b*) 1473603, (*c*) 1573603, and (*d*) 1673603.

calcium fluoride behavior in that interval should be examined. The analysis results indicate that the acceleration of calcium fluoride can be explained by two mechanisms. One is the formation of the eutectic, and the other is the role of calcium and fluorine ions.

A. Kinetics

The raw samples are typically carbon-containing pellets, mainly made of magnesia and carbon. The reaction process of carbon-containing pellets is always described by the unreacted shrinking core model, and the status of vacuum carbothermic reaction of magnesia, in Figure 2, is consistent with the unreacted shrinking core model, so the model is used for data fitting.[14,15] In the model, for spherical particles, the relationship between the time and reaction rate is given depending on the rate-limiting step: chemical reaction, diffusion through the product layer, or combination of reaction and diffusion.

When the first-order chemical reaction function, $f(\beta) = (1 - \beta)^{\frac{2}{3}} - 1$, is plotted against time, a linear fit indicates that chemical reaction is the controlling step. In Figure 8, the plots from bottom to top have, respectively, the regression coefficients of 0.9754,
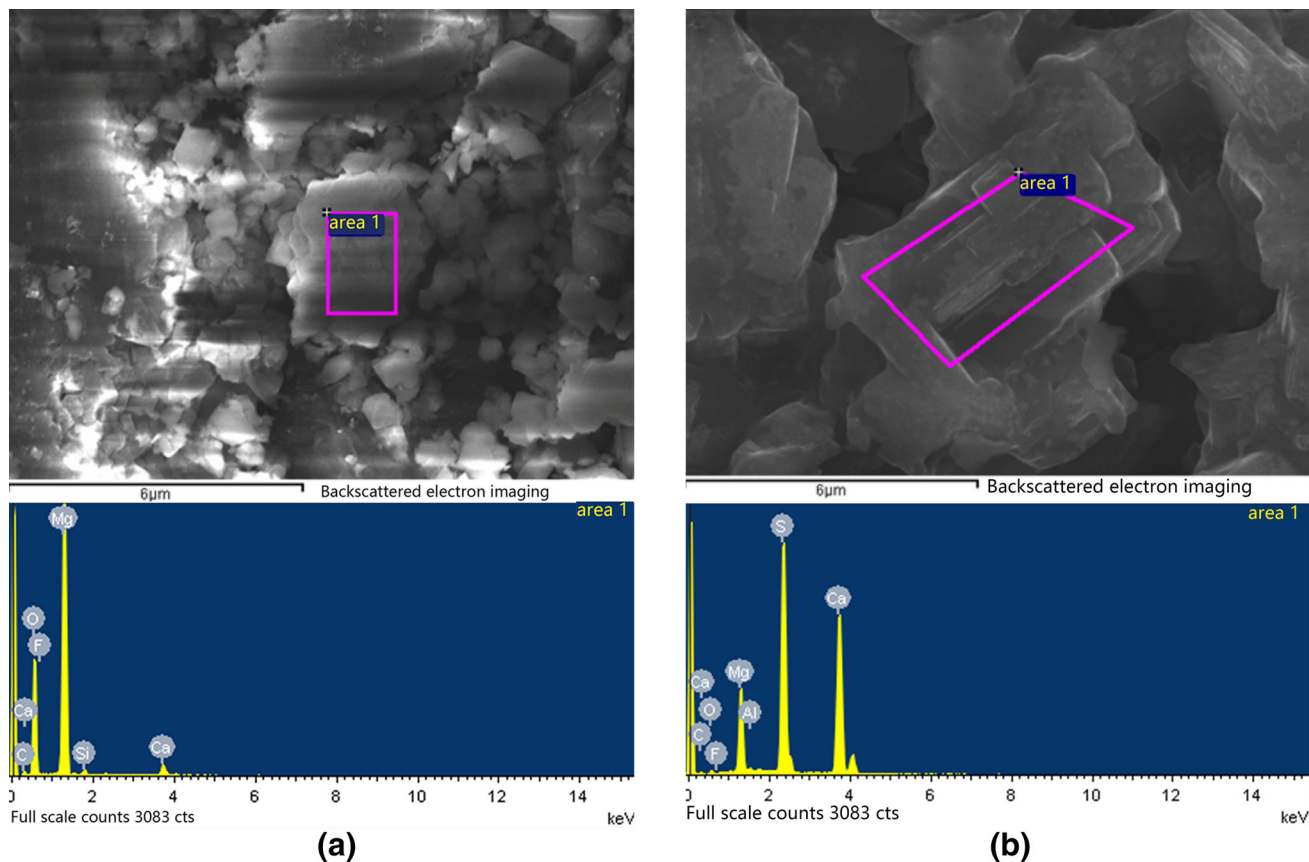
Fig. 7—Detected areas in the electron images and elemental analysis spectra. (*a*) 1473603 and (*b*) 1573603.

Table IV. Element Content Analysis of the Marked Macro-Area

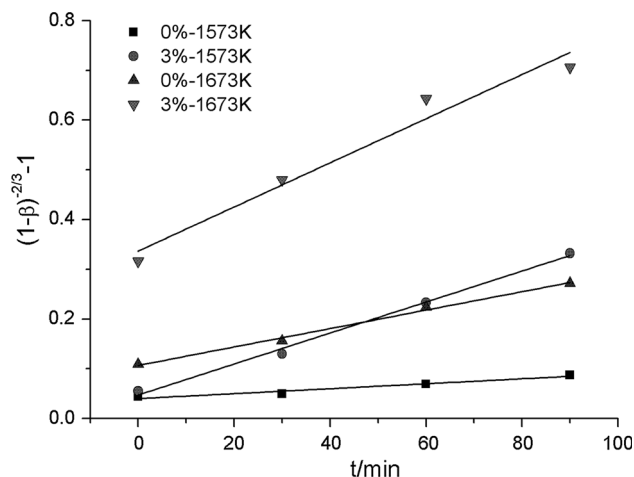| Reaction Condition [K (°C)]	Element	C	Mg	O	Ca	F	Si	Al	S
1473 (1200)	at. pct/pct	9.75	40.36	46.74	1.58	0.92	0.65	0.48	0.00
1573 (1300)	at. pct/pct	19.33	14.81	9.35	26.15	0.00	0.00	0.00	29.89

Fig. 8—Curve of $f(\beta) = (1 - \beta)^{\frac{2}{3}} - 1$ against time.

0.9961, 0.9967, and 0.9704. The plot for the sample with 3 pct CaF_2 at 1673 K (1400 °C) inflects after 60 minutes probably because the CaF_2 has been consumed by 92.82 pct, shown in Figure 5. The chemical reaction rate constant, k, is estimated from the linear plots, 0.499, 1.86, 3.12, and 4.45 ($*10^{-3}$), respectively.

Arrhenius equation is $k = Ae^{\frac{E_a}{RT}}$, where k is the reaction rate constant, R is the molar gas constant, A is the pre-exponential factor, and E_a is the apparent activation energy, the minimum energy for a reaction. E_a is 190.9 kJ/mol for the reaction with 3 pct CaF_2 and 401.0 kJ/mol for that without CaF_2. It is obvious that the calcium fluoride decreases the apparent activation energy of carbothermal reduction of magnesia and enhances the reaction speed.

B. *Formation of the Eutectic*

The thermodynamic calculation and XRD patterns also indicate that mullite decomposed and formed spinel

and olivine at 1473 K (1200 °C), as demonstrated in the following chemical equation:

$$Al_6Si_2O_{13} + 3MgO = 3MgAl_2O_4 + 2SiO_2, \quad [3]$$
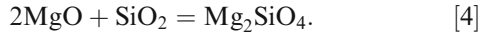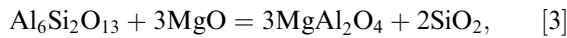
$$2MgO + SiO_2 = Mg_2SiO_4. \quad [4]$$

Of course, the original cristobalite in the coke also reacts as in Eq. [4].

Berezhnoi[16] studied the phase diagram of MgO-SiO$_2$-CaF$_2$ and pointed out that the olivine phase (Mg$_2$SiO$_4$) and calcium fluoride (CaF$_2$) have eutectic temperatures lower than 1473 K (1200 °C) when their molar ratio is approximately 1, which is close to their molar ratio in RS3 (SiO$_2$:CaF$_2$ = 1.08). The olivine phase and calcium fluoride likely generate eutectics in the molten state when the reaction temperature is approximately 1473 K (1200 °C). SEM (Figure 6(c)) and EDS (Figure 7(a)) analyses also indicate that the eutectics were generated. The eutectics in the molten state provide access to this solid–solid reaction process between carbon and magnesia, which was identified in a previous study.[10]

C. Role of Fluorine and Calcium Ions

Calcium fluoride does promote the magnesia reduction by coke, and the two phenomena demonstrate that calcium and fluorine ions work separately. First, for the XRD patterns (Figure 4), CaF$_2$ decreases with increasing temperature for RS1, RS3, and RS5; some silicate phases containing calcium appear, whereas other phases containing fluorine ions do not appear. Second, the EDS (Figure 7) spectra indicate that both calcium and fluorine were present in the eutectic at 1473 K (1200 °C); however, only calcium was present at 1573 K (1300 °C).

Calcium fluoride is a type of ionic compound, and the ionic bond easily breaks in the molten state.[17] Therefore, it could be regarded that the calcium ions and fluorine ions are free in the molten eutectic system at temperatures above 1473 K (1200 °C).

On one hand, the role of fluorine ions is discussed. Fluorine ions and oxygen ions have similar ionic radii of 0.133 and 0.140 nm, respectively, which means that the F$^-$ easily replaced the position of O^{2-} in the magnesia crystal lattice.[18] In addition, F$^-$ is a monovalent ion and O^{2-} is a divalent ion. Two F$^-$ are needed to satisfy the potential to maintain magnesia's electric neutrality. Mirhadi[19] believed that two Si-F bands could replace one Si-O-Si band, which contributed to the breakage of the silica network and the reduction of the stability of the glass structure due to the similarity of ionic radii of fluorine and oxygen. The equilibria are described using the following equations:

$$2MgO + 2F^- = 2MgF^- + O_2 \quad [5]$$

$$MgO + 2F^- = 2MgF_2 + O^{2-}. \quad [6]$$
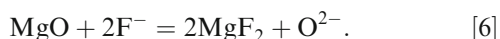
The crystal lattice would be distorted and lead to the decrease of its structural strength and chemical stability; then carbon would easily reduce the unstable magnesia.[20–22]

Sheline[23] confirmed that the molten magnesium fluoride facilitates the decomposition of magnesia by investigating the electrolytic production of Mg from MgO both experimentally and theoretically. Wang[24] provided experimental evidence that magnesium fluoride is generated during the reduction of magnesia with 3 wt pct CaF$_2$. A small addition of ash in the crystallizer near the reaction area was analyzed by XRD, in which the main component was MgF$_2$ (60 to 70 wt pct) with small amounts of CaF$_2$ (0 to 5 wt pct).

Calcium ions also promote the reaction. The appearance of silicate in Figure 4 indicates that calcium ions entered the silicate and replaced the bonded magnesium to be free ions. Then, Ca^{2+} combined the silicate and magnesium ions to form a series of new phases, including olivine, monticellite, and merwinite successively. The calcium ions most likely participate in the following reactions:

$$Ca^{2+} + Mg_2SiO_4 = CaMgSiO_4 + Mg^{2+} \quad [7]$$

$$Ca^{2+} + 2CaMgSiO_4 = Ca_3Mg(SiO_4)_2 + Mg^{2+}. \quad [8]$$
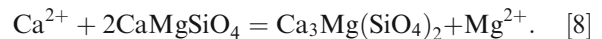
The process releases free magnesium ions to promote the reduction of magnesia by carbon. The replacement consumes both calcium fluoride and olivine, leading to a decrease of the eutectic in the samples. The form of silicate containing calcium and magnesium means the loss of CaF$_2$ and MgO. But the molar ratio of Ca to Mg is 3 in the last stage of merwinite, and the percentage of MgO trapped is up to 1.3 pct for the sample with 5 pct CaF$_2$, which has little impact on MgO reaction rate.

D. Analysis of Loss of Fluorine

Finally, the reason for the fluorine loss is discussed. The fluorine loss is proven by XRF (Figure 5); however, there are no new phases containing fluorine in the residue with decreasing CaF$_2$. This finding indicates that fluorine ions should form some type of gaseous fluoride and be expelled with magnesium vapor and carbon monoxide.

According to Eqs. [5] and [6], magnesium fluoride is generated when fluorine ions destroy the magnesia structure. However, it is volatile under the condition of high temperature and vacuum. Thermodynamic analysis confirms that molten magnesium fluoride evaporation begins at 1556 K (1283 °C) under a vacuum of 10 Pa and at 1602 K (1329 °C) at 20 Pa:

$$MgF_{2(l)} = MgF_{2(g)}. \quad [9]$$
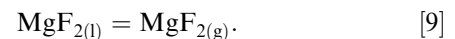
The evaporating temperature is close to 1573 K (1300 °C) and is lower than 1673 K (1400 °C), which corresponds to the increase of the magnesia reaction rate. At 1573 K (1300 °C), magnesium fluoride is generated, thereby accelerating the reaction; however, it evaporates at a relatively low speed. This finding might be the reason that the magnesia reaction rates of RS1, RS3, and RS5 are similar at 1573 K (1300 °C). From 1573 K to 1673 K (1300 °C to 1400 °C), it evaporates faster. RS1, RS3, and RS5 lose fluorine faster, which leads to reaction rates

arranged in the order of the CaF$_2$ weight percentage at 1673 K (1400 °C). At 1673 K (1400 °C), a great loss of fluorine has occurred. The reaction rates increases slowly.

The generation of magnesium fluoride was confirmed by Wang.[24] MgF$_2$ appears in the crystallizer during aluminothermic reduction of dolomite and magnesite with 3 wt pct CaF$_2$ at 1473 K (1200 °C) under a vacuum of 2 Pa.

In addition to the evaporation of magnesium fluoride, the gasification of silicon tetrafluoride is another possible reason leading to the loss of fluorine. The XRF results (Figure 5) show the clear loss of silicon at any temperature, especially at 1673 K (1400 °C). Silicon tetrafluoride easily evaporates or sublimates according to thermodynamic analysis. Viswanathan[25] noted that fluoride in a slag system volatized at 1773 K (1500 °C) and generated SiF$_4$, HF, and CaF$_2$ as gas and dust. Persson[26] studied the fluoride evaporation in three binary MgO-SiO$_2$ systems containing 3 to 10 wt pct CaF$_2$ and noted that fluorine ions enter into the silicate network and SiF$_4$ gas escapes from the molten surface above 1673 K (1400 °C).

Certainly, aluminum fluoride gas and calcium fluoride gas may be generated simultaneously,[27,28]; however, their effects are less pronounced than those of MgF$_2$ and SiF$_4$. The significant loss of fluorine results in the slowdown of reaction rate.

V. CONCLUSIONS

The objective of the work presented here was to determine the acceleration mechanism of calcium fluoride on the vacuum carbothermic reduction of magnesia. Based on the results obtained, the following conclusions can be drawn.

Calcium fluoride and olivine form the eutectic, which forms a channel to aid the solid–solid reaction between carbon and magnesia and facilitates the work of fluorine ions. Fluorine ions are regarded as the critical factor in the acceleration reaction. These ions enter the magnesia crystal lattices through the melt, making them distorted. The structural strength and chemical stability of the magnesia crystal lattice decrease, which facilitates the reduction reaction between carbon and magnesia. Calcium ions replace magnesium ions to form silicate. The gasification of magnesium fluoride and silicon tetrafluoride leads to the loss of fluorine in the samples.

The addition of calcium fluoride promotes the vacuum carbothermal reduction of magnesia. However, the fluoride in the atmosphere results in serious pollution and a series of environmental problems. Maintaining the reduction temperature at approximately 1573 K (1300 °C) could reduce the evaporation of fluoride and keep the reaction relatively faster.

ACKNOWLEDGMENTS

OPEN ACCESS

REFERENCES

1. M. Pourabdoli, S. Raygan, H. Abdizadeh, and K. Hanaei: *Rare Met. Mater. Eng.*, 2006, vol. 35, pp. 74–77.
2. L.Z. Xiong, Q.Y. Chen, Z.L. Yin, P.M. Zhang, Z.Y. Ding, and Z.X. Liu: *Adv. Mater. Res.*, 2012, vol. 22, pp. 694–99.
3. S.Y. Zhong, M.F. Jiang, and H.T. Xu: *Adv. Mater. Res.*, 2012, vols. 347–353, pp. 1180–83.
4. X.M. Li, S.J. Wang, J.X. Zhao, Y.R. Cui, and Y.M. Chen: *Adv. Mater. Res.*, 2011, vols. 239–242, pp. 1960–63.
5. Y.W. Dong, Z.H. Jiang, Y.L. Cao, A. Yu, and D. Hou: *Metall. Mater. Trans. B*, 2014, vol. 45B, pp. 1315–24.
6. Q.Y. Liu, L.Y. Wang, K. Zheng, and H.P. Li: *Ionics*, 2015, vol. 21, pp. 749–53.
7. L.Z. Xiong, Z.Q. He, and Z.X. Liu: *Vacuum*, 2015, vol. 119, pp. 163–67.
8. H.H. Jung, Y. Chung, and J.H. Park: *Metall. Mater. Trans. B*, 2015, vol. 46B, pp. 1154–61.
9. S. Ramakrishnan and P. Koltun: *Resour. Conserv. Recycl.*, 2004, vol. 42, pp. 49–64.
10. Y. Jiang, H.W. Ma, and Y.Q. Liu: *Light Met.*, 2013, vol. 03, pp. 40–53.
11. R.T. Li, P. Wei, and S. Masamichi: *Metall. Mater. Trans. B*, 2003, vol. 34B, pp. 433–37.
12. Y. Tian, T. Qu, B. Yang, Y.N. Dai, B.Q. Xu, and S. Geng: *Metall. Mater. Trans. B*, 2012, vol. 43B, pp. 657–61.
13. J.C. Gao, X.H. Chen, and Q.F. Tang: *J. Funct. Mater.*, 2012, vol. 43, pp. 1312–15.
14. H. Mizoguchi, H. Suzuki, and S. Hayashi: *ISIJ Int.*, 2011, vol. 51 (8), pp. 1247–54.
15. C.H. Huang, C.L. Lin, and H.K. Chen: *J. Chin. Inst. Chem. Eng.*, 2007, vol. 38, pp. 143–49.
16. A.S. Berezhnoi: *Dopov. Akad. Nauk Ukr. RSR*, 1951, vol. 4, pp. 248–52.
17. Y. Sasaki and M. Iguchi: *ISIJ Int.*, 2009, vol. 49 (4), pp. 602–04.
18. R.D. Shannon: *Acta Cryst.*, 1976, vol. A32, pp. 751–67.
19. B. Mirhadi and B. Mehdikhani: *Process. Appl. Ceram.*, 2012, vol. 6, pp. 159–64.
20. M. Backhaus-Ricoult: *Acta Mater.*, 2001, vol. 49, pp. 1747–58.
21. S. Nasr, E.B. Salem, H. Boughzal, and K. Bouzouita: *Ann. Chim. Sci. Mater.*, 2011, vol. 36, pp. 159–76.
22. S. Nasr, A. Hassine, and K. Bouzouita: *J. Biomater. Nanobiotechnol.*, 2013, vol. 4, pp. 1–11.
23. W. Sheline, L. Matthews, N. Lindeke, S. Duncan, and R. Palumbo: *Energy*, 2013, vol. 51, pp. 163–70.
24. Y.W. Wang, J. You, N.X. Feng, and W.X. Hu: *J. Vac. Sci. Technol.*, 2012, vol. 32, pp. 889–95.
25. N.N. Viswanathan, S. Fatemeh, D. Sichen, and S. Seetharaman: *Steel Res.*, 1999, vol. 70, pp. 53–58.
26. M. Persson and S. Seetharaman: *ISIJ Int.*, 2007, vol. 47, pp. 1711–17.
27. M.O. Suk and H.J. Park: *J. Am. Ceram. Soc.*, 2009, vol. 92 (3), pp. 717–23.
28. J.X. Zhao, Y.M. Chen, X.M. Li, Y.R. Cui, and X.T. Lu: *J. Iron Steel Res. Int.*, 2011, vol. 18(10), pp. 24–28, 53.